SIAM J. Applied Dynamical Systems
Vol. 17, No. 2, pp. 1766–1785

Euler Versus Lagrange: The Role of Coordinates in Practical Evans-Function Computations*

Blake Barker†, Jeffrey Humpherys†, Gregory Lyng‡, and Kevin Zumbrun§

Abstract. The Evans function has become a standard tool in the mathematical study of nonlinear wave stability. In particular, computation of its zero set gives a convenient numerical method for determining the point spectrum of the associated linear operator (and thus the spectral stability of the wave in question). We report on an unexpected complication that frustrates this computation for viscous shock profiles in gas dynamics. Although this phenomenon—related to the choice of Eulerian or Lagrangian coordinate system used to describe the gas—is present already in the one-dimensional setting, its implications are especially important in the multidimensional case where no computationally viable Lagrangian description of the gas is readily available. We introduce new "pseudo-Lagrangian" coordinates that allow us to overcome this difficulty, and we illustrate the utility of these coordinates in the setting of isentropic gas dynamics in two space dimensions.

Key words. Evans function, viscous shock profile, stability

AMS subject classifications. 65N25, 34L16, 35L65

DOI. 10.1137/17M113770X

1. Introduction.

1.1. Overview.

The modern theory for the stability of nonlinear waves employs a combination of tools from functional analysis and from dynamical systems, and the Evans function is a key link between these two mathematical disciplines; see, e.g., [1, 28, 39, 41]. In this paper, we describe an unexpected obstacle to Evans-function computations for viscous profiles in gas dynamics. This obstacle arises from the Eulerian coordinate system used to describe the motion of the gas, in combination with the mixed hyperbolic-parabolic nature of the equations. In particular, it does not occur in the parabolic or higher-order systems occurring in reaction diffusion or solitary wave contexts; see Remark 4.3.

While the phenomenon arises even in a single space dimension, it has so far been missed due to the use by practitioners of the somewhat simpler Lagrangian equations. However, in multiple space dimensions, Lagrangian coordinates become impractical due to complexity/introduction of spurious modes [38], and the issue becomes central [24]. Thus, the

*Received by the editors July 7, 2017; accepted for publication (in revised form) by K. Promislow April 11, 2018; published electronically June 19, 2018.
http://www.siam.org/journals/siads/17-2/M113770.html
Funding: The work of the first author was partially supported by NSF grant DMS-1400872. The work of the second author was partially supported by NSF grant DMS-0847074. The work of the third author was partially supported by NSF grants DMS-0845127 and DMS-1413273. The work of the fourth author was partially supported by NSF grant DMS-0801745.
†Department of Mathematics, Brigham Young University, Provo, UT 84602 (blake@mathematics.byu.edu, jeffh@math.byu.edu).
‡Department of Mathematics, University of Wyoming, Laramie, WY 82071 (glyng@uwyo.edu).
§Department of Mathematics, Indiana University, Bloomington, IN 47405 (kzumbrun@indiana.edu).

resolution we describe here—a set of "pseudo-Lagrangian" coordinates—appears to be a crucial component of any successful multidimensional Evans-function computations for viscous shocks in gas dynamics (and related models).

To begin, we briefly describe the abstract mathematical setting in the one-dimensional case. To that end, consider a system of conservation laws with viscosity in a single space dimension. This is a system of partial differential equations of the form

$$U_t + F(U)_x = (B(U)U_x)_x\,. \tag{1.1}$$

In system (1.1), the unknown $U = U(x,t)$ is in $\mathbb{R}^n$, the flux F is a function from $\mathbb{R}^n$ to itself, and the viscosity matrix B is an $\mathbb{R}^{n\times n}$-valued function on $\mathbb{R}^n$. Our motivating example of such a system is the Navier–Stokes equations of gas dynamics; observe that both the Eulerian formulation (2.1) and the Lagrangian formulation (2.8) have the form of (1.1). A viscous shock profile is a traveling-wave solution of (1.1) connecting constant states $U_\pm$. That is, it is a solution of the form

$$U(x,t) = \bar U(x-st)\,,\quad \lim_{z\to\pm\infty}\bar U(z) = U_\pm\,. \tag{1.2}$$

By shifting to a moving coordinate frame, we may assume that the speed s is zero. Thus, the (now) standing-wave solution $\bar U(x)$ is a steady solution of (1.1). To investigate the stability of this wave, we first linearize about it to obtain an equation that approximately describes the evolution of a small perturbation V:

$$V_t = LV := (B(x)V_x)_x - (A(x)V)_x\,, \tag{1.3}$$

where

$$B(x) := B(\bar U(x))\quad\text{and}\quad A(x)V := \mathrm{d}F(\bar U(x))V - \mathrm{d}B(\bar U(x))\big(V,\bar U'(x)\big)\,.$$

The goal, then, is to determine the point spectrum of the variable coefficient (but asymptotically constant) operator L. To that end, we recast the eigenvalue problem $\lambda W = LW$ as a first-order system

$$Z' = \mathbf{A}(x;\lambda)Z\,, \tag{1.4}$$

where the prime denotes differentiation with respect to the spatial variable x, and $Z\in\mathbb{C}^N$ (the size of N depends on the structure of the system (1.1)). Since the point spectrum of L in the unstable half plane is made up of those values λ_* for which there is a nontrivial solution $Z(x;\lambda_*)$ of (1.4) which satisfies

$$\lim_{x\to\pm\infty} Z(x;\lambda_*) = 0\,,$$

these values can be detected by the vanishing of a Wronskian $D(\lambda)$, known as the Evans function. More precisely, since $\bar U$ tends to constant states as $x\to\pm\infty$, there are limiting matrices

$$\mathbf{A}_\pm(\lambda) := \lim_{x\to\pm\infty}\mathbf{A}(x;\lambda)\,.$$

For this introductory discussion, we suppose that for $\lambda \in \{z \in \mathbb{C} : \operatorname{Re} z > 0\}$—the unstable half plane, the dimension of the stable subspace S_+ of $\mathbf{A}_+$ is k and that the dimension of the unstable subspace U_- of $\mathbf{A}_-$ is $N-k$. Then, the Evans function is constructed by building analytic (with respect to λ) bases of solutions

$$\{z_1^+(x;\lambda),\dots,z_k^+(x;\lambda)\} \quad \text{and} \quad \{z_{k+1}^-(x;\lambda),\dots,z_N^-(x;\lambda)\}$$

spanning the manifolds of solutions of (1.4) that tend to zero at each spatial infinity. These bases are built by initializing at the spatial infinities with data from S_+ and U_- and then integrating (1.4) toward $x = 0$. Then, the Evans function is defined to be

$$D(\lambda) := \det(z_1^+,\dots,z_k^+,z_{k+1}^-,\dots,z_N^-)|_{x=0}\,. \tag{1.5}$$

It is evident from this construction that a zero of D corresponds to the existence of a solution of (1.4) which decays at both spatial infinities, i.e., an eigenfunction.

It follows that the computation of D (and, in particular, its zero set) is a central component of the stability analysis. However, for even modestly complicated systems in a single space dimension, this is a task that must be done numerically. Fortunately, this is a computational problem that is by now well understood, and a variety of techniques and algorithms appear in the literature. Starting with a system of form (1.4), the numerical approximation of D essentially consists of two tasks. First, one must compute analytic bases of S_+ and U_-. Second, one must solve the differential equation (1.4) on sufficiently large intervals $[0, M_+]$ and $[-M_-, 0]$. There is a kind of stiffness (when $k \neq 1$ and $N-k \neq 1$) associated with this second problem due to the need to resolve modes of differing exponential decay (growth) rates in order to track the entire subspace of decaying (growing) solutions. A now standard solution to this problem is to work in the exterior product space so that the desired subspace appears as the single maximally stable (unstable) mode. An early example of this kind of numerical computation for solitary-wave solutions of a Boussinesq-type equation can be found in the paper of Alexander and Sachs [2]. For viscous shock profiles, such as discussed above, the program of numerically approximating D using exterior products was initiated and developed by Brin [14, 15, 16]. Bridges and collaborators [3, 13] independently rediscovered this method and clarified its relationship to the earlier compound-matrix method of Ng and Reid [34, 35, 36, 37] for stiff ordinary differential equations (ODEs). Two key later discoveries by Humpherys and Zumbrun [27] and by Humpherys, Sandstede, and Zumbrun [26] helped open the door to large-scale Evans-function computations such as arise in complicated physical problems. The issue is that the exterior-product method, while elegant, does not scale well as N grows. Humpherys and Zumbrun [27] proposed an "analytic orthogonalization" technique which allows for a much more efficient representation of the growing/decaying subspaces. In related work dealing with the other computational task, Humpherys, Sandstede, and Zumbrun [26] proposed an efficient numerical algorithm, based on Kato's projection method [29], that is suitable for computing analytic bases of S_+ and U_- when k and $N-k$ are large. (In practice, it is typical that $k \sim N/2$.) More recent developments include alternative approaches to tackle the problem of large systems [30, 31] and techniques for root-following as parameters vary [25].

As the preceding discussion indicates, there is now a robust collection of numerical methods associated with approximating the Evans function. One culmination of this development

is the STABLAB package [9], a MATLAB-based suite of routines that implements both the exterior-product method and the analytic-orthogonalization method (among other features). Using STABLAB, computational Evans-function techniques have been applied to gas dynamics in one space dimension [5, 6, 21, 22], combustion in one space dimension [7, 19, 23], and magnetohydrodynamics in one space dimension [10]. A recent development is the use of rigorous numerical calculations to establish numerical proofs of spectral stability [4, 11]. This latter development is of particular interest since spectral stability—more precisely, a condition stated in terms of an Evans function which includes spectral stability—is known to imply nonlinear stablity for viscous shock profiles in a variety of hyperbolic-parabolic systems; see, e.g., [32, 33, 41, 42].

In this paper, we focus on a practical issue that arises in the computation of $D(\lambda)$ for physical systems like the Navier–Stokes equations ((2.1) or (2.8)). The main message is a cautionary tale in that a natural coordinate system may not be the "best" one. That is, while Eulerian coordinates are often used in the computational fluid dynamics community (for direct numerical simulations of the flow), *we find that these coordinates lead to an Evans function that is practically incomputable* for intermediate frequencies and moderate shock strengths. In particular, we find that the output of the Eulerian Evans function varies dramatically, both in modulus and argument. Since stability calculations are usually done by winding number counts on the image of a semiannular contour in the unstable complex half plane, rapid changes in modulus and argument lead to computations that are prohibitively complicated and expensive. In particular, this leaves physical models with many parameters and virtually any multidimensional problem out of reach. Thus, despite the existence of mature packages, i.e., STABLAB, for Evans-function computations, one cannot simply feed a coefficient matrix **A** into a package and "hope for the best."

1.2. Multidimensional formulation. The Eulerian-coordinates-based obstacle is present in both one and several spatial dimensions. However, in a single space dimension, the issue can easily be sidestepped by working with the Lagrangian form of the equations. In multiple space dimensions, however, this maneuver is not available, and one must confront the issue head on. Thus, although the main analysis of this paper takes place in a single space dimension, we now outline the general set-up for the multidimensional case as a preliminary to the calculations in section 5, where we illustrate the effectiveness of our pseudo-Lagrangian coordinates for two-dimensional isentropic gas dynamics. Indeed, we expect that our findings will be critical for Evans-based analysis of problems in multidimensional magnetohydrodynamics and detonation theory.

Generalizing (1.1), consider now a system of n conservation laws with viscosity in d space dimensions:

$$f^0(U)_t + \sum_{j=1}^{d} f^j(U)_{x_j} = \sum_{j,k=1}^{d} (B^{jk}(U)U_{x_k})_{x_j}\,. \tag{1.6}$$

In (1.6), $x = (x_1, \dots, x_d) \in \mathbb{R}^d$, $t \in \mathbb{R}$, and $U \in \mathbb{R}^n$ with

$$f^j : \mathbb{R}^n \to \mathbb{R}^n\,, j = 0, 1, \dots, d\,; \quad B^{jk} : \mathbb{R}^n \to \mathbb{R}^{n\times n}\,, j, k = 1, \dots, d\,.$$

We write $A^j(U) := \mathrm{d}f^j(U)$ for $j = 0, 1, \dots, d$.

As above, our interest is in the stability of planar viscous shock profiles. Thus, we consider traveling-wave solutions of the form

$$U(x,t) = \bar{U}(x_1 - st)\,, \quad \lim_{z\to\pm\infty} \bar{U}(z) = U_\pm\,, \tag{1.7}$$

and, without loss of generality, we assume $s = 0$. Similarly as above, we linearize about the steady solution $\bar{U}$ to obtain a linear equation for a small perturbation $V = V(x,t)$. That equation is

$$A^0(x_1)V_t + \sum_{j=1}^{d} (A^j(x_1)V)_{x_j} = \sum_{j,k=1}^{d} (B^{jk}(x_1)V_{x_k})_{x_j}\,, \tag{1.8}$$

where

$$\begin{aligned} A^0(x_1) &:= A^0(\bar{U}(x_1))\,,\\ A^j(x_1)V &:= A^j(\bar{U}(x_1))V - \mathrm{d}B^{j1}(\bar{U}(x_1))\big(V, \bar{U}'(x_1)\big)\,,\\ B^{jk}(x_1) &:= B^{jk}(\bar{U}(x_1))\,. \end{aligned}$$

We take the Laplace transform in time (dual variable λ) and Fourier transform (dual variable $\xi = (\xi_2, \dots, \xi_d)$) in the transverse spatial directions $(x_2, \dots, x_d)$, and we find the generalized eigenvalue equation (supressing the dependence of the coefficients on x_1)

$$\begin{aligned} \lambda A^0 W + (A^1 W)' + \sum_{j=2}^{d} \mathrm{i}\xi_j A^j W = (B^{11}W')' + \sum_{k=2}^{d} (\mathrm{i}\xi_k B^{1k} W)' \\ + \sum_{j=2}^{d} \mathrm{i}\xi_j B^{j1} W' - \sum_{j,k=2}^{d} \xi_j \xi_k B^{jk} W\,. \end{aligned} \tag{1.9}$$

In (1.9), $W = W(x_1, \lambda, \xi)$ represents the transformed perturbation. As above, we reformulate the eigenvalue problem (1.9) as a first-order system of differential equations

$$Z' = \mathbf{A}(x_1; \lambda, \xi) Z\,. \tag{1.10}$$

Here, $\mathbf{A}$ is an $N \times N$ matrix where the dimension N depends on the structure of the system (1.6),[1] and since $\bar{U}$ decays rapidly to its limiting values $U_\pm$ as $x_1 \to \pm\infty$, then the coefficient matrix $\mathbf{A}$ also has constant (with respect to x_1) limiting values. We denote these by $\mathbf{A}_\pm(\lambda, \xi)$.

Remark 1.1 (flux coordinates). A systematic way to formulate the first-order system (1.10) is to use one of the variations of flux coordinates [8]. These coordinates confer concrete benefits for the numerical approximation of the Evans function and are especially useful for multidimensional problems [24].

[1] We have omitted any mention of structural hypotheses on the system (1.6).

Then, as above, the Evans function is built out of the subspaces of solutions of (1.10) which grow at $-\infty$ and decay at $+\infty$; the construction of these subspaces starts with an analysis of the constant-coefficient limiting systems $Z' = \mathbf{A}_{\pm}(\lambda, \xi)Z$. That is, if the collection $\{z_1^+, \dots, z_k^+\}$ forms a basis for the set of solutions of (1.10) that decay at $+\infty$ and, similarly, $\{z_{k+1}^-, \dots z_N^-\}$ spans the set of solutions that deacy at $-\infty$, the Evans function can be written as

$$D(\lambda, \xi) := \det(z_1^+, \dots, z_k^+, z_{k+1}^-, \dots z_N^-)|_{x_1=0}\,. \tag{1.11}$$

Thus, D is a function of frequencies,

$$D : \{\lambda \in \mathbb{C} \,:\, \operatorname{Re}\lambda > 0\} \times \mathbb{R}^{d-1} \to \mathbb{C}\,,$$

whose zeros correspond to eigenvalues, and the principal goal is to compute D (or its zero set).

1.3. Outline. In section 2 we recall the fundamentals of the Eulerian and Lagrangian coordinate systems for gas-dynamical models. For simplicity and concreteness, we carry out these calculations in one space dimension and in the setting of isentropic gas dynamics. Next, in section 3 we describe the two Evans functions arising from the pair of coordinate systems and illustrate their performance, again in the setting of one-dimensional isentropic gas dynamics. In section 4 we describe the mathematical origin of the observed discrepancy in behavior between the Eulerian and Lagrangian Evans functions. We turn to the multidimensional case in section 5, and we introduce there a "pseudo-Lagrangian" Evans function. This Evans function is based on Eulerian coordinates but shares the favorable properties of the one-dimensional Lagrangian Evans function. We illustrate the performance of this new Evans function by considering planar viscous shocks in two-dimensional isentropic gas dynamics. Finally, in section 6, we collect our findings and discuss their implications.

2. Eulerian versus Lagrangian coordinates.

We recall that in continuum physics there are two distinct ways to describe the motion of a fluid. The Eulerian description assigns values to points in the physical domain; thus, $\rho(x,t)$ is the density of the fluid particle that occupies the location x at the instant t. The Lagrangian description is based on an initial labeling of all the fluid particles at some initial instant and tracking them as the fluid moves. Thus, $\tau(y,t) := \rho(y,t)^{-1}$ represents the specific volume at the instant t of the fluid particle marked with the label y. We begin by reviewing the Eulerian and Lagrangian descriptions of viscous shocks.

2.1. Eulerian coordinates. The one-dimensional isentropic Navier–Stokes equations in Eulerian coordinates are

$$\rho_t + (\rho u)_x = 0\,, \tag{2.1a}$$

$$(\rho u)_t + (\rho u^2 + p(\rho))_x = u_{xx}\,, \tag{2.1b}$$

where we have, without loss of generality, set the coefficient of viscosity to be 1. For definiteness, we assume a polytropic, or "γ-law," pressure law

$$p(\rho) = a\rho^{\gamma}, \qquad a, \gamma > 0\,. \tag{2.2}$$

This is not important for our main conclusions, but this assumption streamlines and simplifies the surrounding discussion.

As noted above, a viscous shock is an asymptotically constant traveling-wave solution of (2.1). That is, it is a solution of the form

$$\rho(x,t) = \bar{\rho}(x-\sigma t)\,, \quad u(x,t) = \bar{u}(x-\sigma t)$$

connecting constant states $(\rho_\pm, u_\pm)$. That is, the viscous shock satisfies

$$\lim_{z\to\pm\infty} (\bar{\rho}(z), \bar{u}(z)) = (\rho_\pm, u_\pm)\,.$$

Due to Galilean invariance, without loss of generality, we may assume that the traveling wave of interest is stationary. That is, the wave speed σ is zero. This reduces the traveling-wave equation to the time-independent part of (2.1), namely (dropping bars and using prime to denote differentiation with respect to x)

$$(\rho u)' = 0\,, \quad (\rho u^2 + p(\rho))' = u''\,. \tag{2.3}$$

Integrating (2.3) from $-\infty$ to $+\infty$, we obtain the Rankine-Hugoniot jump conditions

$$[\rho u] = 0\,, \qquad [\rho u^2 + p(\rho)] = 0\,, \tag{2.4}$$

where $[\cdot]$ denotes the difference between limits at $+\infty$ and $-\infty$. It is straightforward to verify that, for a γ-law gas, for each pair of endstates $(\rho_\pm, u_\pm)$ obeying (2.4), there exists a unique heteroclinic connection corresponding to a traveling wave. More, for each choice of momentum flux $m := \rho_\pm u_\pm$, it can be seen that there is a unique solution of (2.4), hence a unique associated stationary shock.

2.2. Lagrangian coordinates. To convert to Lagrangian coordinates, we set

$$y(x,t) = \int_{x^*(t)}^{x} \rho(z,t)\,\mathrm{d}z$$

with $x^*(0) = 0$, $\frac{\mathrm{d}x^*}{\mathrm{d}t} = u(x^*(t),t)$. Then, we observe that

$$\frac{\partial y}{\partial x}(x,t) = \rho(x,t) \tag{2.5}$$

and

$$\begin{aligned}
\frac{\partial y}{\partial t}(x,t) &= \int_{x^*(t)}^{x} \frac{\partial \rho}{\partial t}(z,t)\,\mathrm{d}z - \rho(x^*(t),t)\frac{\mathrm{d}x^*}{\mathrm{d}t} \\
&= -\int_{x^*(t)}^{x} \partial_z(\rho u)\,\mathrm{d}z - \rho(x^*(t),t)u(x^*(t),t) \\
&= -\rho(x,t)u(x,t) + \rho(x^*(t),t)u(x^*(t),t) - \rho(x^*(t),t)u(x^*(t),t) \\
&= -\rho u(x,t)\,. \qquad (2.6)
\end{aligned}$$

Thus, defining

$$\tau(y(x,t),t) = \frac{1}{\rho(x,t)}\,, \quad w(y(x,t),t) = u(x,t), \tag{2.7}$$

and denoting by P the pressure as a function of specific volume, we find—using (2.5) and (2.6)—that the Lagrangian formulation of system (2.1) is

$$\tau_t - w_y = 0\,, \tag{2.8a}$$

$$w_t + P(\tau)_y = \left(\frac{w_y}{\tau}\right)_y. \tag{2.8b}$$

Remark 2.1. Note that this change of coordinates involves both dependent and independent variables; see, e.g., Courant and Friedrichs [17] or Serre [40] for further details.

From (2.8), the traveling-wave equation for a traveling-wave solution of form

$$\tau(y,t) = \bar\tau(y-st)\,, \quad w(x,t) = \bar w(y-st)$$

with $\lim_{\zeta\to\pm\infty}(\bar\tau(\zeta),\bar w(\zeta)) = (\tau_\pm, w_\pm)$ is thus

$$-s\tau' = w'\,, \quad -sw' + P(\tau)' = (w'/\tau)'\,. \tag{2.9}$$

Here, $'$ denotes differentiation with respect to $\zeta := y - st$. Integrating from $-\infty$ to $+\infty$, we obtain the Lagrangian version of the Rankine–Hugoniot conditions (2.4):

$$-s[\tau] - [w] = 0\,, \quad -s[w] + [P(\tau)] = 0\,. \tag{2.10}$$

Using $\rho_+u_+ = \rho_-u_- = m$, we may rewrite the jump condition as

$$m[u] = -[p] = -[P] = -s[w]\,, \tag{2.11}$$

whence $m = -s$. This relation is useful in comparing Eulerian versus Lagrangian shock parametrizations without appealing to the full coordinate transformation.

3. Evans functions and their performance.

We now construct the Evans function in Eulerian and Lagrangian coordinates following [8], and we compare their respective performances. Using the invariances of γ-law gas dynamics [21], we take without loss of generality $m = -s = 1$ and $\rho_- = 1$ in what follows, parametrizing the strength of the shock by u_+ (τ_+) in the Eulerian (Lagrangian) case, where—as above—$\pm$ subscripts denote limits at $\pm\infty$ of corresponding coordinates.

3.1. Eulerian case.

Linearizing (2.1) about a steady profile $(\bar\rho,\bar u)$, we obtain the eigenvalue problem

$$\lambda\rho + (\bar\rho u + \rho\bar u)' = 0\,, \tag{3.1a}$$

$$\lambda(\bar\rho u + \rho\bar u) + (\rho\bar u^2 + 2u + p'(\bar\rho)\rho)' = u''\,. \tag{3.1b}$$

Defining

$$\beta := \frac{\bar{u}^2 + p'(\bar{\rho})}{\bar{u}} \quad \text{and } f := \begin{pmatrix} -\rho\bar{u} - \bar{\rho}u \\ u' - 2u - \beta\bar{u}\rho \end{pmatrix}$$

we may rewrite the eigenvalue problem as the first-order system

$$\begin{pmatrix} f \\ u \end{pmatrix}' = \begin{pmatrix} -\lambda/\bar{u} & 0 & -\lambda\bar{\rho}/\bar{u} \\ -\lambda & 0 & 0 \\ -\beta & 1 & 2 - \beta\bar{\rho} \end{pmatrix} \begin{pmatrix} f \\ u \end{pmatrix}, \tag{3.2}$$

or, briefly,

$$\frac{\mathrm{d}}{\mathrm{d}x} W = \mathbf{A}(x;\lambda) W\,, \quad \text{where} \quad W = \big(f, u\big)^T\,. \tag{3.3}$$

Eigenvalues of (3.1) correspond to values of λ for which there exist solutions of (3.3) decaying as $x \to \pm\infty$, that is, a nontrivial intersection of the manifolds of solutions decaying at $\pm\infty$. By standard asymptotic results from ODEs—e.g., the "gap Lemma" of [18])—one finds that these manifolds are spanned by bases $\{W_1, W_2\}$ and $\{W_3\}$ asymptotic to eigenmodes $\mathrm{e}^{\mu_j x} V_j$ of the stable (unstable) subspaces of the limiting coefficient matrices $\mathbf{A}_\pm := \mathbf{A}(\pm\infty;\lambda)$, where μ_j, V_j depend on λ. The Evans function associated with (3.1) is then defined as

$$D_{\mathrm{E}}(\lambda) := \det(W_1, W_2, W_3)|_{x=0}. \tag{3.4}$$

Here, an important detail is the specification of the "initializing basis vectors at $\pm\infty$" V_j; these are defined as solutions of Kato's ODE [29]

$$\mathrm{d}R/\mathrm{d}\lambda = (\mathrm{d}\mathcal{P}/\mathrm{d}\lambda)R, \tag{3.5}$$

where $\mathcal{P}(\lambda)$ is the (uniquely determined) projection onto the stable (unstable) subspace of $\mathbf{A}_\pm(\lambda)$, and R is a matrix whose columns are the basis vectors V_j.

This determines the Evans function uniquely up to a constant factor, which is then normalized by setting $D_{\mathrm{E}}(\lambda_*) = 1$ at some convenient initializing frequency λ_* (typically the maximum real value of frequencies under consideration). It may be checked that the above definition makes sense, i.e., the counts of stable/unstable basis elements are correct, on the unstable region $\mathrm{Re}\,\lambda \geq 0$, $\lambda \neq 0$, where dimensions of stable/unstable subspaces of $\mathbf{A}_\pm$ agree.

3.2. Lagrangian case. The eigenvalue equation in Lagrangian coordinates is

$$\begin{aligned} \lambda\tau + \tau' - u' &= 0, \\ \lambda u + u' - (P'(\bar{\tau})\tau)' &= \left(\frac{u'}{\bar{\tau}} - \frac{\bar{u}'\tau}{\bar{\tau}^2}\right)', \end{aligned} \tag{3.6}$$

where $\mathsf{P}'(\bar{\tau}) = a\gamma\bar{\tau}^{-\gamma-1}$. This may evidently be written as the first-order system

$$\begin{pmatrix} \tau \\ u \\ u' \end{pmatrix}' = \begin{pmatrix} -\lambda & 0 & 1 \\ 0 & 0 & 1 \\ \lambda\alpha\bar{\tau} & \lambda\bar{\tau} & \bar{\tau}(1-\alpha) \end{pmatrix} \begin{pmatrix} \tau \\ u \\ u' \end{pmatrix} \tag{3.7}$$

or

$$\frac{\mathrm{d}}{\mathrm{d}y}Z = \mathbf{B}(y;\lambda)Z\,, \quad \text{where} \quad Z = \begin{pmatrix}\tau & u & u'\end{pmatrix}^T\,, \tag{3.8}$$

where $\alpha := P'(\bar\tau) - \frac{\bar u'}{\bar\tau^2}$; equivalently one may follow the more complicated, but in this case unnecessary, prescription of [8]. The Lagrangian Evans function $D_{\mathrm{L}}(\lambda)$ is then defined, similarly as in the Eulerian case, as

$$D_{\mathrm{L}}(\lambda) := \det(Z_1, Z_2, Z_3)|_{y=0}, \tag{3.9}$$

where the stable (unstable) manifolds of the flow of (3.8) at $+\infty$ ($-\infty$) are spanned by bases $\{Z_1, Z_2\}$ and $\{Z_3\}$ asymptotic to eigenmodes $\mathrm{e}^{\nu_j y}U_j$ of the stable (unstable) subspaces of the limiting coefficient matrices $\mathbf{B}_\pm := \mathbf{B}(\pm\infty;\lambda)$, with U_j prescribed via Kato's ODE

$$\mathrm{d}S/\mathrm{d}\lambda = (\mathrm{d}\mathcal{Q}/\mathrm{d}\lambda)S, \tag{3.10}$$

where $\mathcal{Q}(\lambda)$ is the (uniquely determined) projection onto the stable (unstable) subspace of $\mathbf{B}_\pm(\lambda)$, and S is a matrix whose columns form the bases U_j. Again, the above prescription is well-defined on the unstable region $\mathrm{Re}\,\lambda \geq 0$, $\lambda \neq 0$.

3.3. Numerical performance. Despite the apparent similarity of Evans functions D_{E} and D_{L}, their performance is quite different for practical computations. These computations typically consist of winding number computations on the image under the Evans function of a semiannular contour determined (by energy estimates or auxiliary asymptotic ODE estimates) to contain all possible unstable eigenvalues of the linearized operator about the wave. A winding number of zero thus corresponds to spectral stability, while a nonzero winding number signals the presence of unstable eigenvalues and therefore instability.

In Figure 1, we plot a traveling-wave solution of (2.1) and the Evans function, evaluated on a semiannulus (see Figure 2(b)) with inner radius $r = 10^{-3}$ and outer radius $R = (1/2 + \sqrt{\gamma})^2$, as computed with the Eulerian coordinates formulation given in (3.2), (3.3). The Evans function maps contours of the form shown in Figure 2(b) to contours of the form shown in Figure 2(c). To compute the Evans function, we use the method of continuous orthogonalization described in [27]. All computations are carried out in STABLAB [9]. We note that in Eulerian coordinates, the Evans function contour wraps around the origin 10 times before unwrapping to yield winding number zero. Further, the Evans function varies over 12 orders of magnitude (from 1 to approximately 2.8e12). This is in stark contrast to the Evans function in Lagrangian coordinates, which is bounded away from the origin and remains order one in modulus (varying from 1 to about 0.2). In Figures 2(a)–(d), we plot the profile solution to (2.8) and the Evans function, evaluated on a semiannulus with inner radius $r = 10^{-3}$ and outer radius $R = (1/2 + \sqrt{\gamma})^2$, as computed with the Lagrangian coordinates formulation given in (3.7). One can see by mere observation that the contour featured in Figures 2(c) and (d) has a winding number of zero.

To summarize, in comparison with the Lagrangian Evans function, the Eulerian Evans function exhibits excessive winding. This makes spectral computations prohibitively complicated and expensive in the Eulerian formulation (as noted earlier, a serious problem in the multidimensional case).

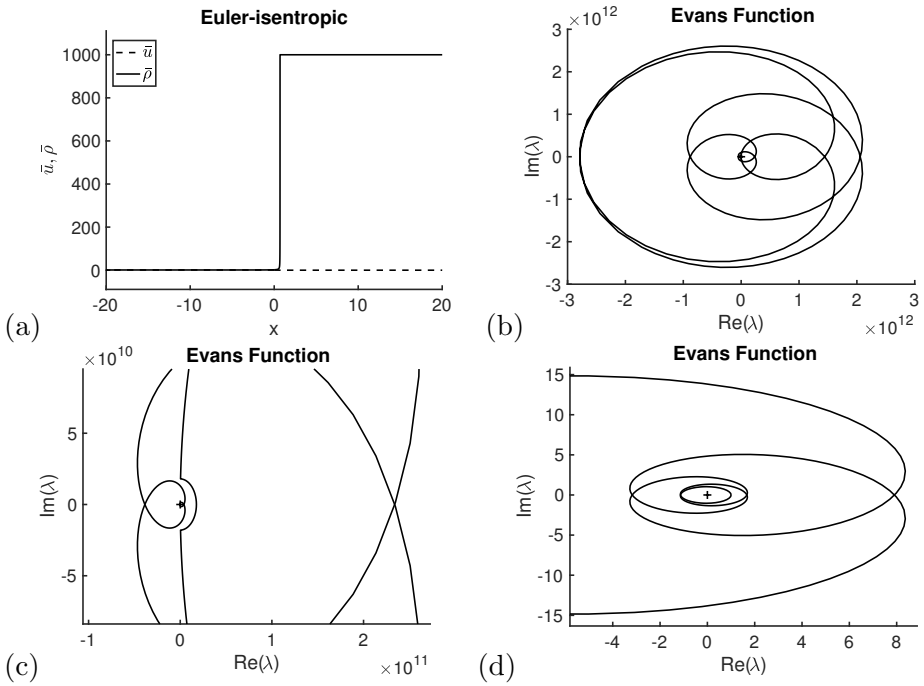

Figure 1. *Plot of the profile and Evans function for one-dimensional isentropic gas in Eulerian coordinates when* $\gamma = 5/3$ *and* $u_+ = 0.001$. (a) *Traveling wave profile.* (b) *Evans function evaluated on a semiannulus contour with inner radius* $r = 10^{-3}$ *and outer radius* $R = (1/2 + \sqrt{\gamma})^2$. (c) *Zoom-in of* (b). (d) *Zoom-in of* (c). *Throughout, a + marks the origin.*

4. Explanation of observed results. We now investigate the origins of the discrepancy between the Eulerian and Lagrangian Evans functions. Evidently, the flows of the Evans systems (3.2) and (3.7) are conjugate; hence, noticing that we have normalized so that $y(0) = 0$, *up to the initialization at* $\pm\infty$, we observe that the two Evans functions should agree up to a nonzero constant factor equal to the determinant at $x = y = 0$ of the λ-independent coordinate transformation between (f, u) and (τ, u, u'). Thus, the discrepancy can only originate from two sources:

(i) the prescription of $V_j(\lambda)$ via Kato's ODE, or
(ii) the asymptotic prescription $W_j \sim e^{\mu_j(\lambda)} V_j(\lambda)$ as $x \to \pm\infty$.

4.1. The conjugating transformations. The relationship between dependent coordinates is given, linearizing the relation $\rho = \tau^{-1}$, by the pair of transformations

$$\begin{pmatrix} \rho \\ u \\ u' \end{pmatrix} = \begin{pmatrix} -\frac{1}{\bar{\tau}^2} & 0 & 0 \\ 0 & 1 & 0 \\ 0 & 0 & 1 \end{pmatrix} \begin{pmatrix} \tau \\ w \\ w' \end{pmatrix}$$

and

$$\begin{pmatrix} f \\ u \end{pmatrix} := \begin{pmatrix} -\bar{u}\rho - \bar{\rho}u \\ u' - 2u - \beta\bar{u}\rho \\ u \end{pmatrix} = \begin{pmatrix} -\bar{u} & -\bar{\rho} & 0 \\ -\beta\bar{u} & -2 & 1 \\ 0 & 1 & 0 \end{pmatrix} \begin{pmatrix} \rho \\ u \\ u' \end{pmatrix},$$

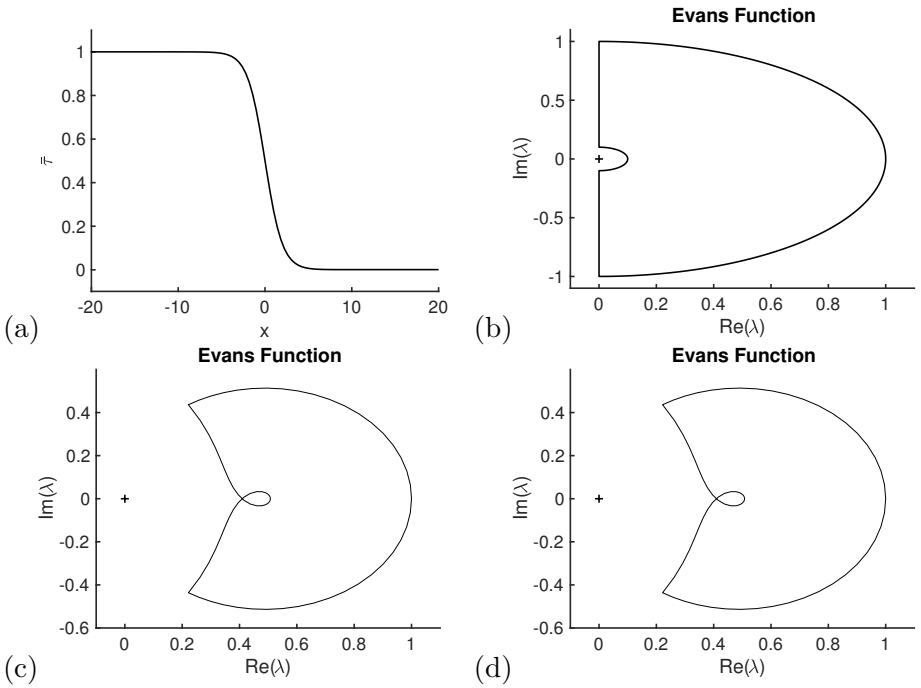

Figure 2. *Plot of the profile and Evans function for one-dimensional isentropic gas in Lagrangian and pseudo-Lagrangian coordinates when* $\gamma = 5/3$ *and* $u_+ = 0.001$. (a) *Profile in Lagrangian coordinates.* (b) *Example of the type of semiannulus contour on which we compute the Evans function.* (c) *Evans function in Lagrangian coordinates.* (d) *Evans function in pseudo-Lagrangian coordinates. Throughout, a* + *marks the origin.*

the composition of which gives a λ-*independent conjuagator* $T(x)$ such that

$$\begin{pmatrix} f \\ u \end{pmatrix} = T(x) \begin{pmatrix} \tau \\ w \\ w' \end{pmatrix}. \tag{4.1}$$

The relation between independent variables is likewise λ-*independent*, given (see (2.5)) by

$$\mathrm{d}y/\mathrm{d}x = \bar{\rho}(x). \tag{4.2}$$

Combining these two observations, the relation between (3.3) and (3.8) is thus

$$\mathbf{B}(y(x);\lambda) = \bar{\rho}(x)^{-1} T(x)^{-1} \mathbf{A}(x;\lambda) T(x). \tag{4.3}$$

4.2. Invariance of Kato's equation. Having observed the λ-independence of the conjugating transformations, we may eliminate the possibility (i) as a source of discrepancy between the two Evans function formulations based on the following general result.

Lemma 4.1. *Kato's ODE is invariant under* λ*-independent coordinate changes.*

Proof. Focusing on either $x = +\infty$ or $x = -\infty$, it is sufficient by (4.3) to consider constant coefficient matrices $\mathbf{A}$, $\mathbf{B}$, related by $\mathbf{B} = \rho^{-1} T \mathbf{A} T^{-1}$, $\mathcal{Q} = T\mathcal{P}T^{-1}$, where $\mathcal{P}$ and $\mathcal{Q}$ are projections onto the stable (unstable) subspaces of $\mathbf{A}$ and $\mathbf{B}$, with $\rho \in \mathbb{R}$ and $T \in \mathbb{R}^{3\times 3}$ constant. Then, the Kato ODEs for the two systems are

$$\mathrm{d}R/\mathrm{d}\lambda = (\mathrm{d}\mathcal{P}/\mathrm{d}\lambda)R \tag{4.4}$$

and

$$\mathrm{d}S/\mathrm{d}\lambda = (\mathrm{d}\mathcal{Q}/\mathrm{d}\lambda)S, \tag{4.5}$$

and the claim is that $S := TR$ is a solution of (4.5) if and only if R is a solution of (4.4). Computing $S' = TR' = T\mathcal{P}'R = T\mathcal{P}'T^{-1}S = \mathcal{Q}'S$, we are done. ∎

4.3. Asymptotic prescription of basis elements. Having eliminated possibility (i), we now explicitly relate the Eulerian and Lagrangian Evans functions by examination of (ii). On the unstable region $\operatorname{Re}\lambda \geq 0$, $\lambda \neq 0$, where our prescriptions of the Evans functions are well-defined, let ν_+ denote the sum of the stable (negative real part) eigenvalues of $\mathbf{A}_+$ and ν_- the sum of the unstable (positive real part) eigenvalues of $\mathbf{A}_-$. Define constants

$$\Delta_+ := \int_0^{+\infty} (\bar\rho(x) - \rho_+)\,\mathrm{d}x \quad \text{and} \quad \Delta_- := \int_{-\infty}^0 (\bar\rho(x) - \rho_-)\,\mathrm{d}x\,. \tag{4.6}$$

Lemma 4.2. *For T as in (4.1), the Eulerian and Lagrangian Evans functions are related by*

$$D_{\mathrm{E}}(\lambda) = \det T(0)\mathrm{e}^{\nu_+\Delta_+ - \nu_-\Delta_-} D_{\mathrm{L}}(\lambda), \tag{4.7}$$

where, for $m = -s = 1$,

$$\nu_+\Delta_+ - \nu_-\Delta_- = -\lambda\Delta_+ + O(\lambda^{1/2}) \quad \textit{as} \quad |\lambda| \to \infty\,.$$

Proof. For T as in (4.1), we have evidently

$$\begin{aligned} D_{\mathrm{E}}(\lambda) &= \det(W_1, W_2, W_3)|_{x=0} \\ &= \det(T\hat Z_1, T\hat Z_2, T\hat Z_3)|_{y=0} \\ &= \det T(0)\det(\hat Z_1, \hat Z_2, \hat Z_3)|_{y=0} \\ &= C(\lambda)\det T(0) D_{\mathrm{L}}(\lambda)\,, \end{aligned}$$

where $C(\lambda)$ is the product of the ratios between bases $\hat Z_j = T^{-1}W_j$ of stable and unstable manifolds and the basis elements $Z_j \sim \mathrm{e}^{\nu_j y}U_j$ prescribed in the definition of the Lagrangian Evans function, or, equivalently, of basis elements $W_j \sim \mathrm{e}^{\mu_j x}V_j$ and TZ_j.

By Lemma 4.1, $TZ_j \sim \mathrm{e}^{\nu_j y(x)}V_j$, whereas, by (4.3), $\mu_j = (\mathrm{d}y/\mathrm{d}x)|_{\pm\infty}\nu_j$. Thus, the ratio $|TZ_j|/|W_j|$ is given by

$$\exp\left(\nu_j \lim_{x\to\pm\infty}(y(x) - x(\mathrm{d}y/\mathrm{d}x))\right).$$

Using $y(0) = 0$, we obtain $y(x) = \int_0^x (\mathrm{d}y/\mathrm{d}x)(z)\,\mathrm{d}z$, hence

$$y(x) - x(\mathrm{d}y/\mathrm{d}x) = \int_0^x \big((\mathrm{d}y/\mathrm{d}x)(z) - (\mathrm{d}y/\mathrm{d}x)(x)\big)dz.$$

Substituting $\mathrm{d}y/\mathrm{d}x = \bar\rho(x)$, and taking the limit as $x \to \pm\infty$, we obtain the result. The asymptotics for $\nu_\pm$ are readily obtained by spectral perturbation analysis, or by asymptotic analysis of the characteristic polynomials of $\mathbf{B}_\pm$, in the limit as $|\lambda| \to \infty$. ∎

For the chosen pressure law and parameters, $\bar\rho$ is increasing, hence $\Delta_\pm < 0$. Moreover, $\Delta_+ < 0$ and $\Delta_- > 0$, hence $D_{\rm E}(\lambda)/D_{\rm L}(\lambda) \sim {\rm e}^{\lambda|\Delta_+|}$, explaining the large difference in winding between images of semicircular contours of large radius under $D_{\rm E}$ versus $D_{\rm L}$.

4.4. High-frequency asymptotics. Lemma 4.2 and the conclusion above explain the large difference between Eulerian and Lagrangian Evans functions, by a factor of order ${\rm e}^{C\lambda}$ as $|\lambda| \to \infty$. However, they do not explain the "goodness" of the Lagrangian version. For this, we appeal to large-λ asymptotics for the individual Evans function, as carried out for the more difficult nonisentropic case in [22, Prop. 4.2], which shows that

$$D_{\rm L}(\lambda) \sim {\rm e}^{C\sqrt{\lambda}} \quad \text{as} \quad |\lambda| \to \infty\,. \tag{4.8}$$

A similar analysis carried out for the Eulerian Evans function gives

$$D_{\rm E}(\lambda) \sim {\rm e}^{C_2\lambda} \quad \text{as} \quad |\lambda| \to \infty\,, \tag{4.9}$$

in agreement with Lemma 4.2. This verifies rigorously the observed phenomenon that the Lagrangian Evans function indeed has much better behavior than the Eulerian version.

More important for our purposes is the asymptotic argument behind the result, which shows that, to leading order as $|\lambda| \to \infty$, the basis elements Z_j "track" the eigendirections of the frozen-coefficient matrix $\mathbf{B}(y,\lambda)$ as y is varied. Thus, their magnitudes r_j obey the simple scalar equations ${\rm d}r_j/{\rm d}y = \nu_j(y) r_j$, where $\nu_j(y)$ are the eigenvalues of the frozen-coefficient matrix $\mathbf{A}(y,\lambda)$, which, taking into account the prescribed asymptotics $r_j \sim {\rm e}^{\nu_j y}$ as $y \to \pm\infty$, results in a magnitude at $y = 0$ of order ${\rm e}^{\int_{\pm\infty}^0 (\nu_j(y) - \nu_j(\pm\infty)dy}$ for each mode.

Among the ν_j, there are two harmless "parabolic" modes $\mu_j \sim \sqrt{\lambda/\bar\tau}$, giving combined contribution $\sim e^{C\sqrt{\lambda}}$. The third, potentially harmful, mode is the "hyperbolic" mode associated with the density equation $\lambda\tau + \tau' = u'$, whose principal part $\lambda\tau = -\tau'$, leads to the eigenvalue

$$\nu_*(y) = -\lambda + O(\lambda^{1/2}).$$

The crucial feature of this eigenvalue is that it is *to leading order constant in* y. Thus, the associated mode Z_* contributes to the Evans function magnitude ${\rm e}^{\int_{\pm\infty}^0 (\nu_*(y) - \nu_*(\pm\infty)dy} \sim {\rm e}^{C\sqrt{\lambda}}$ as $|\lambda| \to \infty$ of the same asymptotic order as the parabolic modes.

For the Eulerian Evans function, on the other hand, the corresponding hyperbolic mode W_* satisfies to leading order the scalar ODE $\lambda\rho + \bar u\rho' = 0$, with an associated eigenvalue

$$\mu_*(x) = -\lambda/\bar u(x) + O(\sqrt{\lambda}) = -(\bar\rho(x)/m)\lambda + O(\sqrt{\lambda})$$

that is *variable coefficient to leading order* in x. This leads to a factor $\sim {\rm e}^{C_1\lambda}$ in the Eulerian Evans function, and the resulting ${\rm e}^{C_1\lambda}$ asymptotics cited above.

Remark 4.3. A similar analysis in the strictly parabolic case arising, for example, in standard reaction diffusion models, or "artificial viscosity" models of compressible gas dymamics, yield favorable high-frequency asymptotics $D(\lambda) \sim {\rm e}^{C\sqrt{\lambda}}$ independent of the choice of coordinate system, and so this issue does not arise. Nor does it arise for third- and higher-order models such as KdV or Boussinesq equations. Indeed, for *semilinear problems* typically studied in these settings, the asymptotics are a still more favorable $D(\lambda) \sim 1$.

5. Pseudo-Lagrangian coordinates: Multiple space dimensions. We turn now to the multidimensional case. We consider the isentropic Navier–Stokes equations in space dimension $d = 2$. In Eulerian coordinates, the system takes the form

$$\partial_t \rho + \operatorname{div}(\rho \mathbf{v}) = 0\,, \tag{5.1a}$$

$$\partial_t(\rho \mathbf{v}) + \operatorname{div}(\rho \mathbf{v} \otimes \mathbf{v}) + \operatorname{grad} p = \mu \Delta \mathbf{v} + (\mu + \eta) \operatorname{grad} \operatorname{div} \mathbf{v}\,, \tag{5.1b}$$

where ρ is density, $\mathbf{v} = (v_1, v_2)$ velocity, p is pressure, related to density by (2.2), and constants μ and η are coefficients of first and second viscosity [12, 24]. Linearizing about a steady planar profile $(\rho, \mathbf{v}) = (\bar\rho, \overline{\mathbf{v}})(x_1)$ varying in the x_1 direction only, without loss of generality $\bar v_2 \equiv 0$, we obtain the eigenvalue equations

$$\lambda \rho + \operatorname{div}(\bar\rho \mathbf{v} + \rho \overline{\mathbf{v}}) = 0\,, \tag{5.2a}$$

$$\begin{aligned} \lambda(\bar\rho \mathbf{v} + \rho \overline{\mathbf{v}}) + \operatorname{div}(\rho \bar{\mathbf{v}} \otimes \bar{\mathbf{v}} + \bar\rho \mathbf{v} \otimes \bar{\mathbf{v}} + \bar\rho \bar{\mathbf{v}} \otimes \mathbf{v}) + \operatorname{grad} p(\bar\rho) \\ = \mu \Delta \mathbf{v} + (\mu + \eta) \operatorname{grad} \operatorname{div} \mathbf{v}\,. \end{aligned} \tag{5.2b}$$

Taking the Fourier transform in x_2, we obtain a family of ODEs in x_1 parametrized by the Fourier frequency ξ. Expressing this as a first-order system, we may define an Evans function

$$D_{\mathrm{E}}(\lambda, \xi) \tag{5.3}$$

similarly as in the one-dimensional case, with zeros corresponding to generalized eigenmodes $\mathrm{e}^{\mathrm{i}\xi x_2} w(x_1)$, w decaying at infinity, associated with eigenvalue λ. See [8, 24] for further details.

This Evans function has equally poor behavior as the one-dimensional version; indeed, for $\xi = 0$, the multidimensional Eulerian Evans function reduces to (a nonvanishing multiple of) the one-dimensional one. However, in contrast to the one-dimensional case, a useful Lagrangian version of the Evans function does not seem to be available; Pogan, Yao, and Zumbrun [38] discuss this issue in some depth.

5.1. Pseudo-Lagrangian coordinates. To resolve this problem, making possible practical multidimensional Evans function computations, we introduce instead a new *pseudo-Lagrangian* formulation of the Evans function, based on the Eulerian version, but sharing the good properties of the one-dimensional Lagrangian Evans function. Namely, dropping the subscript on x_1, and writing the first-order Evans system as

$$\mathrm{d}W/\mathrm{d}x = \mathbf{A}(x; \lambda, \xi) W,$$

we introduce $\mathrm{d}Y/\mathrm{d}y = \mathbf{B}(y; \lambda, \xi) Y$, where $\mathbf{B}$ is defined by $\mathbf{B}(y(x); \lambda, \xi) = (\mathrm{d}x/\mathrm{d}y)\mathbf{A}(x; \lambda, \xi)$, and denote the resulting Evans function by $D_{\mathrm{pL}}(\lambda, \xi)$.

Partial justification for this choice is given by the following straightforward result. Abusing notation somewhat, let $D_{\mathrm{pL}}(\lambda)$ denote the one-dimensional version of the pseudo-Lagrangian Evans function, obtained from the Eulerian Evans system by the change of dependent variable $\mathrm{d}y/\mathrm{d}x = \bar\rho(x)$ as was done in the multidimensional case.

Proposition 5.1. *The one-dimensional pseudo-Lagrangian Evans function $D_{\mathrm{pL}}(\lambda)$ agrees with (i.e., is a constant multiple) of the one-dimensional Lagrangian Evans function $D_{\mathrm{L}}(\lambda)$.*

Proof. This follows by the argument in the proof of Lemma 4.2, but now observing that the Lagrangian and pseudo-Lagrangian flows are conjugate by a change of dependent variables alone, with no change of independent variable. ∎

Further motivation is given by the hyperbolic ρ equation of the Fourier transformed eigenvalue equation,

$$\lambda\rho + (\mathrm{d}/\mathrm{d}x)(\rho\bar{v}_1 + \bar{\rho}v_1) + \mathrm{i}\xi\bar{\rho}v_2 = 0\,,$$

which has principal part $\lambda\rho + \bar{v}_1(\mathrm{d}/\mathrm{d}x)(\rho) = 0$, or $\mathrm{d}\rho/\mathrm{d}x = -\lambda/\bar{v}_1$ as in the one-dimensional case. Thus, $\mathrm{d}\rho/\mathrm{d}y = (\mathrm{d}\rho/\mathrm{d}x)(\mathrm{d}x/\mathrm{d}y) = -(\lambda/m)\rho$, with $m \equiv \bar{\rho}\bar{v}_1$ constant, similarly as in the one-dimensional case. Thus, the corresponding asymptotic eigenvalue $\nu_*(\lambda,\xi)$ of the frozen-coefficient matrix $\mathbf{B}(y;\lambda,\xi)$ is, to leading order, independent of y, and we obtain favorable large-$|\lambda|$ asymptotics also for the multidimensional version of the pseudo-Lagrangian Evans function.

5.2. Numerical performance. As in one dimension, we find that the image of a contour under evaluation of the multidimensional Evans function in Eulerian coordinates wraps excessively around the origin before unwinding again and varies in modulus significantly more than when using pseudo-Lagrangian coordinates. For example, when $\gamma = 5/3$, $u_+ = 0.06$, $\xi = 1$, and we compute the Evans function on a contour like that shown in Figure 2(b), but with inner radius set to $r = 1e-3$ and outer radius to $R = 30$, we find that in Eulerian coordinates it takes 1344 points on the preimage contour in order for the image contour to vary in relative distance no more than 0.2, whereas for pseudo-Lagrangian coordinates, 212 preimage points suffice. As seen in Figure 3, the Evans function computed in Eulerian coordinates varies in

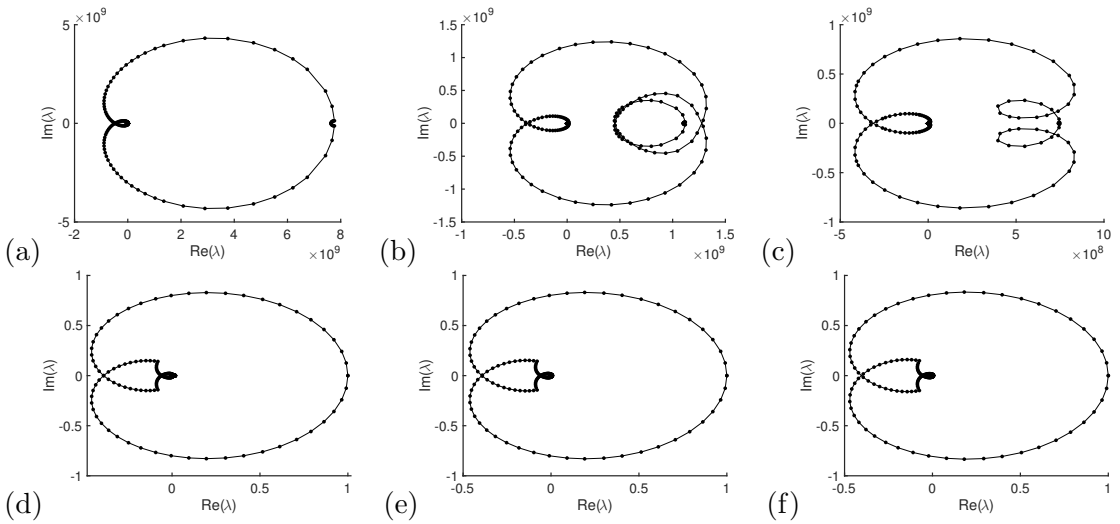

Figure 3. *Evans function output for two-dimensional isentropic gas in Eulerian coordinates (top row) and pseudo-Lagrangian coordinates (bottom row) when $\gamma = 5/3$ and $u_+ = 0.06$. In all figures, the Evans function is evaluated on a semiannulus contour with inner radius $r = 10^{-3}$ and outer radius $R = 30$. The Fourier parameter is $\xi = 0$ in* (a) *and* (d)*, $\xi = 0.5$ in* (b) *and* (e)*, and $\xi = 1$ in* (c) *and* (f)*.*

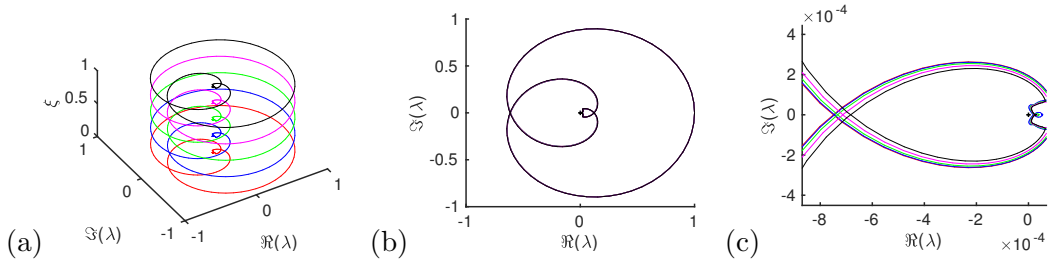

Figure 4. *Pseudo-Lagrangian coordinates and the variation of D with respect to ξ. The figures show three views of the the images of the Evans function for different values of ξ (red, $\xi = 0$; blue, $\xi = 0.25$; green, $\xi = 0.5$; magenta, $\xi = 0.75$; black, $\xi = 1$.) A three-dimensional view is given in* (a)*, a vertical view in* (b)*, and a zoomed-in view near the origin in* (c)*. A black + marks the origin. The parameters are $v_{1+} = 0.06$, $\gamma = 5/3$.*

Table 1

The computational cost of the Eulerian method and pseudo-Lagrangian method. The first two columns indicate the parameter τ_+ and the Fourier variable ξ. The last four columns indicate the number of points and computation time it took to compute the Evans function on a contour of radius $R = 90$ with an adaptive Evans-function evaluator which requires that the relative error between points in the image contour be no greater than 0.2*. In the last four columns a p represents the number of points on which the contour is computed and a t represent the computation time. The subscripts* E *and* pL *stand respectively for the Euler method and the pseudo-Lagrange method.*

τ_+	ξ	p_{E}	t_{E}	p_{pL}	t_{pL}
0.2733	0	238	579.9	112	396
0.2733	0.3	256	466.9	138	368.2
0.2733	0.6	240	458.1	124	357.7
0.22	0	348	983.7	120	386.8
0.22	0.3	376	785.7	150	353.1
0.22	0.6	356	775.1	136	358
0.1667	0	396	1163	184	530.1
0.1667	0.3	440	837.2	218	504.1
0.1667	0.6	422	862.8	200	498.4
0.1133	0	676	1829	206	555.3
0.1133	0.3	702	1612	248	479.1
0.1133	0.6	676	1641	226	486.1
0.06	0	948	2916	340	814.6
0.06	0.3	1012	2566	392	758.7
0.06	0.6	984	2577	378	782.1
0.001	0	12708	3.51e5	740	1224

modulus over three times more orders of magnitude then in pseudo-Lagrangian coordinates. An even starker contrast occurs when the Evans function is computed on a contour with outer radius $R = 90$ and inner radius $r = 1e-3$, but with $\gamma = 5/3$, $\xi = 0$, and $u_+ = 0.001$. The Evans function in Eulerian coordinates takes 4.06 days to compute, varies over 225 orders of magnitude, and requires 12,708 points in order for the image contour to vary in relative distance no more than 0.2, whereas the Evans function in pseudo-Lagrangian coordinates takes 20.4 minutes to compute, varies over 12 orders of magnitude, and requires 740 points. Furthermore, in pseudo-Lagrangian coordinates, the Evans function for multidimensional isentropic gas has small variation as ξ varies. This is shown in Figure 4. Finally, differences in cost (in terms of the number of evaluations required and the computing time) are compiled in Table 1.

The same significant improved performance of pseudo-Lagrangian coordinates manifests itself in the full gas system as well [24]. One other advantage of pseudo-Lagrangian coordinates for isentropic gas is that it requires the traveling wave profile in Lagrangian coordinates and not Eulerian coordinates. For the examples featured in Figure 3, we had to use continuation to solve the profile in Eulerian coordinates as u_+ decreased and eventually solve it as a scalar system using a stiff ODE solver. On the other hand, in Lagrangian coordinates continuation was not needed to solve the profile.

6. Conclusions. Our results illustrate that coordinate choices, at the level of physical models, can have substantial impacts on the viability of a given Evans-function computation. Coupling this with our companion results [8] on the practical role of coordinate choices in the construction of the first-order eigenvalue equation, we see a simple takeaway message: coordinate choices matter. While viscous shock profiles in one space dimension can equally well be described in Eulerian and Lagrangian coordinates, the two Evans functions arising from the two models behave substantially differently, and these differences affect the viability of computations for spectral stability.

The import of coordinate choices goes far beyond minimizing winding for attractive pictures of Evans-function output. For physical systems with many parameters and/or for multidimensional problems, it is essential to minimize the number of function evaluations to have a chance to properly explore parameter and frequency space. Indeed, as noted above, we expect pseudo-Lagrangian coordinates to be necessary for any kind of computational Evans-function analysis of multidimensional problems in magnetohydrodynamics and in detonation theory. More generally, this phenomenon will be present in general composite type hyperbolic-parabolic systems and perhaps in other settings as well.

While the phenomenon is not present in the strictly second and higher-order cases (Remark 4.3), explaining why issues such as the above have not appeared in the extensive Evans-function literature associated with traveling-wave solutions of reaction-diffusion and dispersive equations, it does suggest an interesting and important open problem relevant for general systems. Namely, given a physical system, which representative of the Evans function is the "best" for computational purposes? Since the stability calculations generally involve winding numbers, one measure of "best" might be in terms of minimizing total variation in the argument and perhaps also the modulus of $D(\lambda)$ as λ traverses a typical contour, or some weighted versions thereof. A very interesting direction would be to expand the possible range of dependent and independent coordinate transformations to include also λ-dependent coordinates not considered here, analagous to time-dependent mesh choices considered in the thematically related problem of optimal coordinatization in adaptive mesh control [20].

Certainly the example of gas dynamics presented here suggests that some kind of answer to the above question is required if numerical Evans-function calculations are going to be part of a general purpose, push-button stability calculator. Thus, in addition to recent developments of Evans-function approximations in numerical proofs of stability [4, 11], we see optimizing the computed Evans functions as a central issue in the future development of computational Evans-function techniques.

Acknowledgment. We thank the anonymous referees for their careful reading and several helpful comments improving the exposition.

REFERENCES

[1] J. Alexander, R. Gardner, and C. Jones, *A topological invariant arising in the stability analysis of travelling waves*, J. Reine Angew. Math., 410 (1990), pp. 167–212.

[2] J. C. Alexander and R. Sachs, *Linear instability of solitary waves of a Boussinesq-type equation: A computer assisted computation*, Nonlinear World, 2 (1995), pp. 471–507.

[3] L. Allen and T. J. Bridges, *Numerical exterior algebra and the compound matrix method*, Numer. Math., 92 (2002), pp. 197–232.

[4] B. Barker, *Numerical proof of stability of roll waves in the small-amplitude limit for inclined thin film flow*, J. Differential Equations, 257 (2014), pp. 2950–2983.

[5] B. Barker, J. Humpherys, O. Lafitte, K. Rudd, and K. Zumbrun, *Stability of isentropic Navier-Stokes shocks*, Appl. Math. Lett., 21 (2008), pp. 742–747.

[6] B. Barker, J. Humpherys, K. Rudd, and K. Zumbrun, *Stability of viscous shocks in isentropic gas dynamics*, Comm. Math. Phys., 281 (2008), pp. 231–249.

[7] B. Barker, J. Humpherys, G. Lyng, and K. Zumbrun, *Viscous hyperstabilization of detonation waves in one space dimension*, SIAM J. Appl. Math., 75 (2015), pp. 885–906.

[8] B. Barker, J. Humpherys, G. Lyng, and K. Zumbrun, *Balanced flux formulations for multidimensional Evans-function computations for viscous shocks*, Quart. Appl. Math., 76 (2018), pp. 531–545.

[9] B. Barker, J. Humpherys, J. Lytle, and K. Zumbrun, *STABLAB: A MATLAB-Based Numerical Library for Evans Function Computation*, https://github.com/nonlinear-waves/stablab.git (2017).

[10] B. Barker, J. Humpherys, and K. Zumbrun, *One-dimensional stability of parallel shock layers in isentropic magnetohydrodynamics*, J. Differential Equations, 249 (2010), pp. 2175–2213.

[11] B. Barker and K. Zumbrun, *Numerical proof of stability of viscous shock profiles*, Math. Models Methods Appl. Sci., 26 (2016), pp. 2451–2469.

[12] G. K. Batchelor, *An Introduction to UID dynamics*, 2nd ed., Cambridge Mathematical Library, Cambridge University Press, Cambridge, UK, 1999.

[13] T. J. Bridges, G. Derks, and G. Gottwald, *Stability and instability of solitary waves of the fifth-order KdV equation: A numerical framework*, Phys. D, 172 (2002), pp. 190–216.

[14] L. Q. Brin, *Numerical Testing of the Stability of Viscous Shock Waves*, Ph. D. Thesis, Indiana University, 1998.

[15] L. Q. Brin, *Numerical testing of the stability of viscous shock waves*, Math. Comp., 70 (2001), pp. 1071–1088.

[16] L. Q. Brin and K. Zumbrun, *Analytically varying eigenvectors and the stability of viscous shock waves*, Mat. Contemp., 22 (2002), pp. 19–32.

[17] R. Courant and K. O. Friedrichs, *Supersonic Flow and Shock Waves*, Appl. Math. Sci. 21, Springer, New York, 1976.

[18] R. A. Gardner and K. Zumbrun, *The gap lemma and geometric criteria for instability of viscous shock profiles*, Comm. Pure Appl. Math., 51 (1998), pp. 797–855.

[19] J. Hendricks, J. Humpherys, G. Lyng, and K. Zumbrun, *Stability of viscous weak detonation waves for Majda's model*, J. Dynam. Differential Equations, 27 (2015), pp. 237–260.

[20] W. Huang and R. D. Russell, *Adaptive Moving Mesh Methods*, Appl. Math. Sci., 174, Springer, New York, 2011.

[21] J. Humpherys, O. Lafitte, and K. Zumbrun, *Stability of isentropic Navier–Stokes shocks in the high-Mach number limit*, Comm. Math. Phys., 293 (2010), pp. 1–36.

[22] J. Humpherys, G. Lyng, and K. Zumbrun, *Spectral stability of ideal-gas shock layers*, Arch. Ration. Mech. Anal., 194 (2009), pp. 1029–1079.

[23] J. Humpherys, G. Lyng, and K. Zumbrun, *Stability of viscous detonations for Majda's model*, Phys. D, 259 (2013), pp. 63–80.

[24] J. Humpherys, G. Lyng, and K. Zumbrun, *Multidimensional stability of large-amplitude Navier–Stokes shocks*, Arch. Ration. Mech. Anal., 226 (2017), pp. 923–973, https://doi.org/10.1007/s00205-017-1147-7.

[25] J. Humpherys and J. Lytle, *Root following in Evans function computation*, SIAM J. Numer. Anal., 53 (2015), pp. 2329–2346.

[26] J. Humpherys, B. Sandstede, and K. Zumbrun, *Efficient computation of analytic bases in Evans function analysis of large systems*, Numer. Math., 103 (2006), pp. 631–642.
[27] J. Humpherys and K. Zumbrun, *An efficient shooting algorithm for Evans function calculations in large systems*, Phys. D, 220 (2006), pp. 116–126.
[28] T. Kapitula and K. Promislow, *Spectral and Dynamical Stability of Nonlinear Waves*, Appl. Math. Sci. 185, Springer, New York, 2013.
[29] T. Kato, *Perturbation Theory for Linear Operators*, 2nd ed., Grundlehren Math. Wiss. 132, Springer-Verlag, Berlin, 1976.
[30] V. Ledoux, S. J. A. Malham, and V. Thümmler, *Grassmannian spectral shooting*, Math. Comp., 79 (2010), pp. 1585–1619.
[31] V. Ledoux, S. J. A. Malham, J. Niesen, and V. Thümmler, *Computing stability of multidimensional traveling waves*, SIAM J. Appl. Dyn. Syst., 8 (2009), pp. 480–507.
[32] C. Mascia and K. Zumbrun, *Pointwise Green function bounds for shock profiles of systems with real viscosity*, Arch. Ration. Mech. Anal., 169 (2003), pp. 177–263.
[33] C. Mascia and K. Zumbrun, *Stability of large-amplitude viscous shock profiles of hyperbolic-parabolic systems*, Arch. Ration. Mech. Anal., 172 (2004), pp. 93–131.
[34] B. S. Ng and W. H. Reid, *An initial value method for eigenvalue problems using compound matrices*, J. Comput. Phys., 30 (1979), pp. 125–136.
[35] B. S. Ng and W. H. Reid, *A numerical method for linear two-point boundary value problems using compound matrices*, J. Comput. Phys., 33 (1979), pp. 70–85.
[36] B. S. Ng and W. H. Reid, *On the numerical solution of the Orr-Sommerfeld problem: Asymptotic initial conditions for shooting methods*, J. Comput. Phys., 38 (1980), pp. 275–293.
[37] B. S. Ng and W. H. Reid, *The compound matrix method for ordinary differential systems*, J. Comput. Phys., 58 (1985), pp. 209–228.
[38] A. Pogan, J. Yao, and K. Zumbrun, *$O(2)$ Hopf bifurcation of viscous shock waves in a channel*, Phys. D, 308 (2015), pp. 59–79.
[39] B. Sandstede, *Stability of travelling waves*, in Handbook of Dynamical Systems, Vol. 2, North-Holland, Amsterdam, 2002, pp. 983–1055.
[40] D. Serre, *Systems of Conservation Laws.* 1, *Hyperbolicity, Entropies, Shock Waves*, Cambridge University Press, Cambridge, UK, 1999.
[41] K. Zumbrun, *Stability of large-amplitude shock waves of compressible Navier-Stokes equations*, in Handbook of Mathematical Fluid Dynamics, Vol. 3, North-Holland, Amsterdam, 2004, pp. 311–533.
[42] K. Zumbrun, *Planar stability criteria for viscous shock waves of systems with real viscosity*, in Hyperbolic Systems of Balance Laws, Lecture Notes in Math. 1911, Springer-Verlag, Berlin, 2007, pp. 229–326.